AN ANALYSIS OF DECONVOLUTION: MODELING REFLECTIVITY BY FRACTIONALLY INTEGRATED NOISE

Muhammed M. Saggaf and M. Nafi Toksöz

Earth Resources Laboratory
Department of Earth, Atmospheric, and Planetary Sciences
Massachusetts Institute of Technology
Cambridge, MA 02139

ABSTRACT

Reflection coefficients are observed in nature to have stochastic behavior that departs significantly from the white noise model. Conventional deconvolution methods, however, assume reflectivity to be a white noise process. In this paper we analyze the deconvolution process, study the implications of the assumption of white noise, and show that the conventional operator can recover only the white component of reflectivity. A new stochastic model, fractionally integrated noise, is proposed for modeling reflectivity. This model more closely approximates its spectral character and that encompasses white noise as a special case. We discuss different techniques to generalize the conventional deconvolution method based on the new model in order to handle reflectivity that is not white, and compare the results of the conventional and generalized filters using data derived from well logs.

INTRODUCTION

Conventional deconvolution schemes assume that the earth's reflectivity has a white noise correlation structure. However, reflection coefficients in nature tend to behave in a different manner: generally their power spectra are proportional to frequency (Hosken, 1980; Walden and Hosken, 1985; Todoeschuck *et al.*, 1990; Rosa and Ulrych, 1991).

Figures 1a–f show the power spectra of typical reflectivity logs from four different wells. These were derived from sonic and density logs in various areas of the central and eastern regions of Saudi Arabia and were computed for a plane wave with normal incidence by $r = (\rho_2\nu_2 - \rho_1\nu_1)/(\rho_2\nu_2 + \rho_1\nu_1)$, where ρ_i and ν_i are the density and acoustic velocity in layer i, respectively. The spectra were calculated by FFT analysis on the

samples using the Welch method of power spectrum estimation and a Hanning window. Note how each spectrum has a richer content of high frequencies (sometimes referred to as "blueness," borrowing the term from the visible light spectrum), and appears to be directly proportional to frequency. Such behavior is encountered quite frequently in nature and has been noted over the years. This behavior is sometimes described as quasi-cyclic and blocky layering and can be interpreted as evidence of self-organization and structuring in the crust (Shtatland, 1991).

Reflectivity is thus observed to have spectral behavior that departs significantly from the white noise model. In this paper, we analyze how the assumption of white noise can adversely affect the deconvolution process, propose an alternate model for reflectivity, and suggest techniques to generalize deconvolution to handle the more general case of reflectivity that has a nonwhite correlation structure.

By far the most widely used method of calculating the deconvolution filter is Wiener filtering (Robinson, 1957; Robinson and Treitel, 1967, 1980). Among the other methods are the l_1 norm criterion (Barrodale and Roberts, 1973), Burg's method (Burg, 1975), Kalman filtering (Ott and Meder, 1972), minimum entropy deconvolution (Wiggins, 1978), homomorphic deconvolution (Ulrych, 1971), zero-phase deconvolution, and time-adaptive algorithms (Griffiths *et al.*, 1977). Jurkevics and Wiggins (1984) compared these methods and concluded that Wiener filters are the most robust under a wide variety of input conditions. Wiener deconvolution is sometimes also called least-squares filtering. We will consider optimal Wiener filtering here, though the discussion applies to any form of deconvolution that assumes reflectivity to have white noise correlation and spectral properties.

WHITE NOISE AND FRACTIONALLY INTEGRATED NOISE

A process $\{z_t\}$ is said to be white noise if it consists of uncorrelated random variables. The auto-correlation function of such a process is a simple unit spike and the power spectrum is flat. The process can be Gaussian, but does not have to be so, i.e., being white noise is a description of the correlation structure of the process, not the probability distribution structure.

A process $\{y_t\}$ is said to be fractionally integrated noise of order d (denoted sometimes by the acronym FIN) if its dth differencing is white noise (Hosking, 1981). This process may be written as $\nabla^d y_t = z_t$, where $\{z_t\}$ is a white noise process and the differencing operator ∇^d can be written in terms of the backward shift operator B as $\nabla^d = (1-B)^d$, $By_t = y_{t-1}$. In this definition d does not need to be an integer (fractional differencing), and the fractional differencing operator is defined by its binomial series expansion:

$$\nabla^d = \sum_{k=0}^{\infty} \binom{d}{k} (-B)^k = 1 - dB - \frac{1}{2}d(1-d)B^2 - \frac{1}{6}d(1-d)(2-d)B^3 - \dots . \quad (1)$$

The term "differencing" is used here rather than "derivative" as the process is in-

trinsically defined for discrete-time series, and is not merely an approximation of a continuos-time process. Note that $d = 0$ corresponds to the case of white noise (i.e. zero differencing). The process is stationary for $d < 0.5$ and Gaussian if $\{z_t\}$.

The auto-correlation function ρ_y and power spectrum P_y are given by

$$\rho_y(k) = \frac{\Gamma(1-d)\Gamma(k+d)}{\Gamma(d)\Gamma(k+1-d)} \tag{2}$$

and

$$P_y(f) = \sigma^2 \sqrt{\frac{\Gamma(1-d)}{\Gamma\left(\frac{1}{2}-d\right)}} \sin^{-2d}(\pi f), \tag{3}$$

where σ^2 is the variance, the mean is taken to be zero, f is the frequency normalized by the folding frequency, and Γ is the Gamma function. Figures 2a and 2b show the auto-correlation function and power spectrum of fractionally integrated noise processes of various orders (the auto-correlation at lag zero is always 1 and is not shown).

Fractionally integrated noise can be used to simulate both long-memory and short-memory processes (where memory refers to the span of interdependence between observations) and can thus be adapted to model reflection coefficients ($d < 0$) and acoustic impedance ($d > 0$). Its power spectrum approximates well the characteristics of reflectivity. In addition, the process has analytically calculable auto-correlation and spectral density functions. Moreover, it is extendable to a larger class of processes, namely $ARIMA(p, d, q)$: fractionally integrated auto-regressive moving-average processes (Hosking, 1981). This is a generalization of the process described by Box and Jenkins (1976), where the parameter d was restricted to have integral values. Fractionally integrated noise can therefore also be referred to as $ARIMA(0, d, 0)$.

THE CONVENTIONAL DECONVOLUTION PROCESS

The simplest convolutional model regards the trace as the convolution of the effective seismic wavelet with the earth's reflection coefficients. Reverberatory multiples and propagation effects are often included in this effective wavelet (Robinson, 1985). If we denote the trace by s, the seismic wavelet by w, and reflectivity by r, we have:

$$s = w * r \tag{4}$$

where $*$ denotes the convolution operator.

The goal in deconvolution is to develop a filter f such that when applied to the trace, it recovers the earth's reflectivity behavior. To design the deconvolution operator, a knowledge of the auto-correlation of the wavelet is required. Since that quantity is unknown, conventional schemes assume that reflection coefficients behave as white noise. Since the auto-correlation of the latter process is a spike, this assumption justifies using the auto-correlation of the trace in place of that of the wavelet, as they should be equal

in this case. This assumption is mades the problem more tractable, and is often accepted since the method works sufficiently in many situations.

We now analyze what happens when the reflectivity is not white noise. Consider the trace given by (4). We assume for the time being that the wavelet is minimum-phase (another common assumption in deconvolution, which we will not tackle here). We can always factor reflectivity into a minimum-phase nonwhite-noise component, r_m, and an all-pass component, r_a, that is white noise of some phase, since a minimum-phase equivalent can always be calculated for any signal with a finite, nonvanishing power spectrum:

$$r = r_m * r_a. \tag{5}$$

When reflectivity is not white noise, the minimum-phase component r_m does not vanish. Figure 3a shows a 100-point realization of such reflectivity sampled at 4 ms, while Figures 3b and 3c show its minimum-phase and all-pass components, respectively. Such factorization can be done by calculating the minimum-phase version of reflectivity and then deconvolving to get the all-pass component by dividing it by the frequency domain. The minimum-phase version can be found by least squares, by performing FFT (noting that the phase spectrum of a minimum-phase signal equals the Hilbert transform of the logarithm of the amplitude spectrum), or by factoring the polynomial of the z-transform and projecting the roots outside the unit circle. Although in practice these techniques do not always give identical outcomes due to the limited operator length of the least squares method and the finite FFT series length of the Hilbert transform method, equivalent results can be obtained with adequate choice of parameters. Figure 3d shows the power spectrum of the full reflectivity and the spectrum of a fractionally integrated noise process of order -0.8 (dashed). Figure 3e shows the power spectrum of the all-pass component of reflectivity. We note that it is indeed white (flat), unlike that of the full reflectivity.

The conventional deconvolution operator is the inverse of the minimum-phase component of the trace. Thus, it acts as a discriminator that removes the nonwhite minimum-phase component from the trace. Since, by assumption, the wavelet is minimum-phase, the minimum-phase component of the trace is thus the convolution of the wavelet with the minimum-phase component of reflectivity. This can be stated in another way by noting that since r_a is white, we have:

$$\begin{aligned} ac(s) &= ac(w * r_m * r_a) \\ &= ac(w * r_m) \\ \Rightarrow \quad f &= (w * r_m)^{-1}, \end{aligned} \tag{6}$$

where ac denotes the auto-correlation function. For prediction error deconvolution (gap deconvolution), the filter operator is the same as that of spiking deconvolution but smoothed by the leading part of the inverse of the spiking filter (up to the gap length). Therefore, the same argument made above applies, except that a smoothing operator is applied afterwards to the output.

Applying the conventional deconvolution filter to the trace, we get:

$$\begin{aligned} f * s &= f * w * r_m * r_a \\ &= [f * (w * r_m)] * ra \\ &= r_a. \end{aligned} \tag{7}$$

Thus, we see that conventional deconvolution does not recover the full reflectivity; it recovers only its white all-pass component. Thus, the output of the conventional filter is often white. That the output is white should not be taken, however, to indicate that reflectivity itself is white. As we have just shown, it should only mean that the conventional deconvolution filter can recover only the white component of reflectivity. In effect, our assumption of whiteness has biased the filter to produce an output that conforms to that assumption. We should therefore expect that a better model for reflectivity other than white noise would give rise to a better deconvolution filter.

Figures 4a and 4b show, respectively, a trace produced from the reflectivity of Figure 3a and the minimum-phase wavelet that was used to produce that trace. Figures 4c and 4d show the reflectivity recovered from the trace by conventional deconvolution and the power spectrum of that reflectivity, respectively. Comparing with Figures 3c and 3e, we see that the output of conventional deconvolution is essentially the same as the all-pass component of true reflectivity. In other words, conventional deconvolution fails to recover the nonwhite component of reflectivity, and the RMS (*root-mean-square*) error in this case between the true and recovered reflectivity series is 43%. The RMS error is defined here as:

$$\text{RMS error} = \frac{\sum_t (e_t - r_t)^2}{\sum_t e_t^2} \tag{8}$$

where $\{e_t\}$ is the exact reflectivity series and $\{r_t\}$ is the recovered reflectivity series (the output of the deconvolution filter).

Figures 4e and 4f show the reflectivity recovered by a generalized version of deconvolution and the power spectrum of that reflectivity, respectively. We discuss this method in the next section. For now, we note that in this case, the deconvolution operator was able to recover the full reflectivity, not just its white component; the match is almost perfect (compare with Figures 3a and 3d), with only a 9% RMS error.

RESIDUAL WAVELET

The residual wavelet is a popular method for measuring the effectiveness of deconvolution when the true reflectivity is known. It is most often calculated by dividing the recovered reflectivity series by the true one in the frequency domain (Jurkevics and Wiggins, 1984). The residual wavelet can thus be represented as:

$$w_r = r_r * r^{-1}, \tag{9}$$

where r_r is the recovered reflectivity. Therefore, we have:

$$\begin{aligned} w_r &= f * s * r^{-1} \\ &= f * w * r * r^{-1} \\ &= f * w. \end{aligned} \tag{10}$$

Conventional analysis hence considers the spikeness of the residual wavelet as a measure of how effectively the deconvolution operator removes the wavelet. This view would be correct if reflectivity were white. However, since the seismic wavelet in this case is minimum-phase, we would expect the deconvolution operator to approximate the inverse of the wavelet to a much better degree than is indicated by the residual wavelet as calculated by either the usual method (9) or by (10), shown in Figures 5a and 5b, respectively. In fact, the width of the residual wavelet here is comparable to that of the first lobe of the seismic wavelet, indicating that deconvolution has done a poor job of compressing the seismic wavelet.

The reason for this inconsistency is explained as follows. Since reflectivity is not white, the conventional deconvolution operator, being a discriminator for white noise, removes not only the wavelet but also part of the reflectivity as well. Namely, it removes the nonwhite part of reflectivity. Hence, regarding the residual wavelet as a measure of how successful the deconvolution operator in removing the wavelet is only partially correct. Moreover, the degree to which the conventional operator successfully removes the nonwhite component of the trace (an undesirable feat, since this removes the nonwhite part of reflectivity) can be calculated by evaluating $f * w * r_m$. This expression is shown in Figure 5c, and it is a measure of the filter numerical performance as an inverse operator. Indeed, we see that this is almost a perfect spike (compare with Figure 5a).

Let us look at the residual wavelet in a different way:

$$\begin{aligned} w_r &= r_r * r^{-1} \\ &= f * s * r^{-1} \\ &= [f * (w * r_m)] * r_a * r^{-1} \\ &= r_a * r^{-1}. \end{aligned} \tag{11}$$

This is what happens when reflectivity is not white. The deconvolution operator here is actually the inverse of the convolution of the wavelet with the nonwhite component of reflectivity. Indeed, if we calculate the residual wavelet by (11) instead of the usual method (9), we get essentially the same answer, as shown in Figure 5d. Compare that with Figures 5a and 5b. In fact, the differences between Figures 5a,b, and d are primarily due to time windowing effects. In contrast, Figure 5e shows the residual wavelet left by the generalized filter mentioned in the previous section. This is a sharper spike, and is more in line with what we expect deconvolution to do—compress the seismic wavelet.

Hence, for a minimum-phase seismic wavelet, the residual wavelet is actually a measure of how close the all-pass component of reflectivity is to being the true reflectivity. In other words, it is a measure of the whiteness of reflectivity; and in this sense, the

name "residual wavelet" is essentially a misnomer. When the seismic wavelet is not minimum-phase, the meaning of the residual wavelet is a combination of the two views, i.e., it is a measure of the whiteness of reflectivity as well as how close the seismic wavelet is to being minimum-phase. For a more complex convolutional model, it is also a measure of the filter performance in the presence of noise. Nevertheless, regardless of the interpretation we attach to it, the residual wavelet remains a useful tool to gauge the effectiveness of the deconvolution process as a whole, in the sense that it is a benchmark of the difference between the true and recovered reflectivity series.

In short, conventional deconvolution removes part of reflectivity as well as the wavelet, which is obviously undesirable. Also, the residual wavelet depends on how well we model reflectivity, not just on the success of the filter in compressing the seismic wavelet.

CALCULATING THE GENERALIZED DECONVOLUTION OPERATOR

How can we generalize the conventional deconvolution process to handle reflectivity that is not white noise? We first begin by choosing an appropriate model for reflectivity, one that mimics its stochastic behavior to a much better degree than white noise. In this paper, we propose the use of fractionally integrated noise as such a model.

The dashed lines in Figures 1a–f show the power spectrum of the fractionally integrated noise process used to model reflectivity in each of the wells. The order of the process (its single relevant parameter here) can be calculated by a simple fit to the spectrum of the well log data. Alternatively, fitting can also be done in the time domain by a modification to the procedure described by Box and Jenkins (1976) to model *ARMA* processes. That model, however obtained, can then be used to process data in proximate locations. Doing this would be especially convenient if the success of the generalized technique were relatively insensitive to the process order. We will see later that this process indeed seems to be the case. Walden and Hosken (1985) observed reflection coefficients derived from eight well logs to have power spectra that are proportional to frequency according to a power law f^{β}, where $0.5 < \beta < 1.5$. Their observation is consistent with our findings, as (from (3)) the process order d is approximately equivalent to $-\beta/2$; thus we would expect $-0.75 < d < -0.25$, which is the case in the wells we examined (Figures 1a–d).

Conventional deconvolution is inadequate because the assumption of white noise reflectivity is essentially flawed, and thus the auto-correlation of the trace is a rather poor estimate of that of the wavelet. The most obvious way to generalize the conventional deconvolution scheme given a chosen model is to let deconvolution utilize a better estimate of the wavelet auto-correlation. To this end, we can design an optimal least-squares inverse filter g that is the inverse of the minimum-phase component of reflectivity. The design of this filter relies on the model, since the auto-correlation function used to calculate the filter operator is found from (2). We will call this filter

the reflectivity whitening filter since it removes the minimum-phase component of reflectivity and leaves only the white all-pass component. Hence, if reflectivity is given by (5), then we have:

$$g = r_m^{-1}. \tag{12}$$

Therefore, after application of the filter, we have:

$$\begin{aligned} g * s &= g * w * r_m * r_a \\ &= w * r_a. \end{aligned} \tag{13}$$

Since r_a is white, the auto-correlation of the filtered trace is then a good estimate of the auto-correlation of the wavelet.

With this improved estimate of the auto-correlation, we can proceed to calculate the usual deconvolution filter $\hat{f}$ and apply it to the *original* trace (Figure 6e, method 1). From (13) we get:

$$\begin{aligned} ac(g * s) &= ac(w) \\ \Rightarrow \quad \hat{f} &= w^{-1} \\ \Rightarrow \quad \hat{f} * s &= \hat{f} * w * r \\ &= r. \end{aligned} \tag{14}$$

We have denoted this conventional deconvolution filter by $\hat{f}$ to differentiate it from the filter f mentioned previously (defined in (7)) since the two filters are distinct, in general, as they are calculated from different inputs. When the order of the fractionally integrated noise process is zero (i.e., reflectivity is modeled by white noise), the whitening filter is the identity filter, and the filtered trace is unchanged. So, in this special case, the technique reduces to the conventional deconvolution method, as it should.

Figure 6a shows the trace minus the minimum-phase component of reflectivity (i.e., it shows the convolution of the wavelet with the all-pass component of reflectivity). Figure 6b shows the original full trace after application of the whitening filter. The two look similar. Figure 6c shows the power spectrum of reflectivity after application of the whitening filter. Comparing Figure 6c with Figure 3e (the spectrum of the all-pass component of reflectivity), we see that the two look alike; the whitening filter has whitened the reflectivity.

It is instructive to look at the above in the frequency domain also. To get a good estimate of the auto-correlation of the wavelet from the trace, we can whiten the spectrum of the reflectivity component in the trace by dividing the Fourier transform of the trace by the square root of the power spectrum of the model, as given by (3). After that, reflectivity would be whitened, and the modified trace should thus give a good estimate of the auto-correlation of the wavelet. We can then proceed as before by calculating the usual deconvolution operator from the modified trace and applying it to the original trace (Figure 6e, method 2).

We note that the process described here is essentially the same as applying the zero-phase version of the whitening filter. Both this filter and the whitening filter whiten the reflectivity component of the trace. The phase spectrum of the filter is irrelevant here since we are using the filtered trace only to calculate the auto-correlation function (which is independent of phase), and the final deconvolution operator $\hat{f}$ is applied to the original unfiltered trace. Figure 6d shows the power spectrum of reflectivity before and after whitening in the frequency domain.

Both schemes described above require modification of the actual conventional deconvolution code, since the trace passed to the conventional deconvolution step (i.e., the trace filtered by the whitening filter or its zero-phase version) is not the same as the trace to which the final deconvolution operator is to be applied (which is the original trace). It would be useful perhaps to use the existing deconvolution code and modify the above schemes so that they reuse established deconvolution programs. This can be done by applying the whitening filter to the trace, feeding it to an existing conventional deconvolution routine, and then filtering the output by the inverse of the whitening filter (Figure 6e, method 3). From (14) we have:

$$\begin{aligned} g^{-1} * \hat{f} * g * s &= \hat{f} * s \\ &= r. \end{aligned} \tag{15}$$

In this case, it is important that the whitening filter be minimum phase. Otherwise, the conventional deconvolution routine used as part of the technique would produce a sub-optimal result that will not be compensated by the inverse filter. Also, having a minimum-phase filter guarantees that it has a stable inverse.

Even more useful would be a filter that can be applied after conventional deconvolution to restore the nonwhite component of reflectivity that was removed by the conventional deconvolution operator (Figure 6e, method 4). Indeed, this is perhaps the easiest technique to implement and use, though the other three techniques mentioned above shed more light on the inner workings of the generalized deconvolution scheme. Designing such an "after-the-fact" filter is easy enough; it is the inverse of the whitening filter. From (12) we have:

$$g^{-1} = r_m. \tag{16}$$

Hence, by using (7) we get:

$$\begin{aligned} g^{-1} * f * s &= g^{-1} * r_a \\ &= r_m * r_a \\ &= r. \end{aligned} \tag{17}$$

We will call g^{-1} the spectral compensation filter.

The results obtained by using any of the four techniques should be the same, of course. We can see this in Figure 6e, which shows the reflectivity recovered from the trace using the four methods. The results shown previously in Figures 4e, 4f, and 5e were obtained using the spectral compensation filter method.

We mentioned previously that our assumption of the whiteness of reflectivity biased the output of conventional deconvolution into having a stochastic behavior consistent with that assumption. This assumption generalizes and follows directly from (16) and (17) since the compensation filter is essentially the minimum-phase component of reflectivity that has the power spectrum governed by (3). When the order of the fractionally integrated noise model is zero, the compensation filter is the identity filter, and the outcome of deconvolution is white (since r_a is white), just as in the case of conventional deconvolution. For a fractionally integrated noise model of any other order, the final deconvolution output will have a spectrum consistent with that of the compensation filter. In other words, it will have spectral density governed by the particular fractionally integrated noise model used.

In fact, we can generalize further and state that whatever model is utilized (be it fractionally integrated noise, auto-regressive moving-average, scaling Gaussian noise, fractional Brownian motion, or any other model), the final deconvolution outcome will have the spectral density dictated by that model. If instead of using a stochastic model, we use the exact auto-correlation function of reflectivity (say, from a well log) in calculating the whitening filter, the result would lead to a spectral compensation filter that is almost the same as the minimum-phase version of reflectivity, and deconvolution would recover reflectivity almost fully. Figure 7a shows the recovered reflectivity obtained in this case. Note how close the match is to the true reflectivity (Figure 3a). The RMS error here is only 1%, which is mostly due to the numerical inexactness of the 10-point filter used. Figure 7b shows that the residual wavelet left in this case is practically a perfect spike, indicating nearly perfect deconvolution. Of course, away from the well location this does not help us, and the use of stochastic modeling is therefore essential.

In short, the success of deconvolution invariably depends on the model. The conventional method of deconvolution recovers only the white component of reflectivity, the generalized scheme recovers more of reflectivity, as dictated by the model. Using fractionally integrated noise, the conventional method becomes a special case of the generalized one (when the order of the model process is zero). While it may appear that generalizing the conventional scheme adds the burden of a governing stochastic model to be estimated, in actuality, stochastic modeling is implicitly performed even in the conventional method. Conventional deconvolution indeed relies on a stochastic model (white noise), albeit a parameterless (and arguably inadequate) one.

TESTS USING WELL LOG DATA

Here we use reflectivity series derived from sonic and density logs of two wells in Saudi Arabia: well A, on-shore in the central province, and D, an off-shore well in the Gulf. The former is finely sampled at 0.5 ms and the latter is sampled at 2 ms. The reflection coefficients were computed as described in the introduction. The wavelet used to produce the traces has the same shape as that in Figure 4b but it was sampled according to the sampling interval of reflectivity.

The reflection coefficients for well A appear in Figure 8a. Their power spectrum was shown in Figure 1a along with the best-fitting fractionally integrated noise process, which was found to have an order of roughly -0.45. Figures 8c and 8d show, respectively, the reflectivity recovered from the trace (Figure 8b) by the conventional and generalized deconvolution approaches. It can be seen that the one produced by the generalized filter resembles true reflectivity much more closely than that of conventional deconvolution. In fact, the RMS error for the conventional approach is 20% and an error of 1% for the generalized approach. Figures 9a and 9b show the residual wavelet left by the two deconvolution methods. We see that the residual wavelet left by the generalized filter is a much sharper spike than that left by the conventional one, the width of the latter being comparable to that of the first lobe of the seismic wavelet, indicating poor wavelet compression. Therefore, visual inspection, RMS error, and the residual wavelet all show that utilizing a better model for reflectivity than white noise could lead to a significant improvement in the performance of the deconvolution filter.

Figure 9c shows the residual wavelet left by the generalized deconvolution filter for a range of the order of the fractionally integrated noise model. It is encouraging to see that as long as the order of the process is chosen within a reasonable interval (-0.75 to -0.25, say), the generalized filter consistently outperforms the conventional one. Thus, the generalized method is not very sensitive to the order of the fractionally integrated noise model. This is shown even more emphatically in Figure 9d, where the RMS error between the true and recovered reflectivity series is plotted against the order of the fractionally integrated noise process used in constructing the filter. An order of zero corresponds to conventional deconvolution.

Figure 10a shows the reflection coefficients of well D, whose power spectrum appeared in Figures 1e and 1f along with that of the fractionally integrated noise process of order -0.55. Figures 10c and 10d show the reflectivity recovered from the trace (Figure 10b) by the conventional and generalized deconvolution filters, respectively. Again, the similarity to the true series is much closer for the latter. The RMS errors are 25% and 3%, respectively. Figures 11a and 11b show the residual wavelet left by the two deconvolution filters. Figure 11c shows the residual wavelets produced by the generalized method for a varying number of model process orders. Finally, Figure 11d shows the RMS error versus the process order used in constructing the generalized filter.

The same conclusions can be drawn from these figures as before. It would seem, therefore, that an accurate estimate of the fractionally integrated noise model order is not necessary. A rough estimate drawn from a nearby well would be enough to produce a satisfactory improvement in the deconvolution output. This is not surprising, considering that reflection coefficients are observed to deviate from the white noise model to some degree in the majority of cases. Thus, a conservative correction to the white conventional deconvolution output would only bring it closer to the actual reflectivity series.

NONSTATIONARITY

Figures 12a–d show the order of the best-fitting fractionally integrated noise process for a 500-point sliding window along the well logs whose power spectra appear in Figures 1a–d, plotted against the center point of each window. From these figures it can be seen that the stochastic properties of reflectivity seem to change significantly with depth. In other words, strictly speaking, reflectivity is not a stationary time series. Of course, in each case, the average of the orders along the plot is roughly the same as the order of the fractionally integrated noise process used to model the entire data set. However, the character of the variations in the stochastic behavior is distinct for each well: blocky (Figure 12a, where it can be divided into two regions the order in each of the which is mostly constant), parabolic (Figure 12b), monotonically decreasing (Figure 12c), or monotonically increasing (Figure 12d).

Designing a multi-gate generalized deconvolution filter, using fractionally integrated noise models of differing orders for each gate, leads to even better performance. However, the design of such filters would require even more knowledge of the underlying stochastic parameters. It is arguable whether the uncertainty in the estimates of those parameters warrants such a scheme, at least not without further examination of the extent of the lateral variations in the stochastic properties of reflectivity with depth (or dense coverage of logs).

A more interesting issue (one which we do not tackle here) is the correlation between the shape of the plots in Figures 12a–d and the underlying stratigraphic lithology. Perhaps correlating the lithology with the changing stochastic parameters of reflectivity would aid in understanding the geological processes responsible for the nonwhite spectral behavior of reflectivity.

CONCLUSIONS

The deconvolution process relies implicitly on stochastic modeling to recover reflectivity. The model used invariably biases the output of the deconvolution operator to have spectral character consistent with that of the governing model. Conventional deconvolution, using white noise as its model, can recover only the white component of reflectivity, and the rest of reflectivity is removed with the wavelet. Utilizing a model that more closely matches the stochastic behavior of reflectivity observed in nature from well log data thus leads to a deconvolution operator that does a better job of recovering the reflection coefficients from the trace.

We see that by using fractionally integrated noise, the conventional deconvolution process can be generalized to handle reflectivity that departs stochastically from the white noise model; the generalized filter encompasses conventional deconvolution as a special case. Additionally, it appears that an accurate knowledge of the spectral properties of reflectivity is not needed in order for the generalized filter to perform satisfactorily. Thus, estimates of the order of the fractionally integrated noise model

can be drawn from a rough analysis of the stochastic properties of reflectivity derived from well logs in proximate locations.

The nonstationarity of the stochastic properties of reflectivity is an interesting issue for further research, and the correlation with lithology could shed more light on the geological processes responsible for the observed spectral behavior of reflectivity.

ACKNOWLEDGMENTS

Discussions with Enders Robinson and Ernest Shtatland are gratefully acknowledged. M. M. Saggaf was supported by a Saudi Aramco fellowship during part of this research. This work was also supported by the Borehole Acoustics and Logging/Reservoir Delineation Consortia at the Massachusetts Institute of Technology.

REFERENCES

Barrodale, I. and Roberts, F.D.K., 1973, An improved algorithm for discrete l_1 linear approximation, *SIAM J. Num. Anal., 10,* 839–848.

Box, G.E. and Jenkins, G.M., 1976, *Time Series Analysis: Forecasting and Control,* Holden-Day.

Burg, J.P., 1975, Maximum entropy spectral analysis, Ph.D. thesis, Stanford University.

Griffiths, L.J., Smolka, F.R., and Trembly, L.D., 1977, Adaptive deconvolution: A new technique for processing time-varying seismic data, *Geophysics, 42,* 742–759.

Hosken, J.W.J., 1980, A stochastic model for seismic reflections, 50th Ann. Internat. Mtg., Soc. Expl. Geophys., Abstract G-69.

Hosking, J.R.M., 1981, Fractional differencing, *Biometrika, 68,* 165–176.

Jurkevics, A. and Wiggins, R., 1984, A critique of seismic deconvolution methods, *Geophysics, 49,* 2109–2116.

Ott, N. and Meder, H. G., 1972, The Kalman filter as a prediction error filter, *Geophys. Prosp., 20,* 549–560.

Robinson, E.A., 1957, Predictive decomposition of seismic traces, *Geophysics, 22,* 767–778.

Robinson, E.A., 1985, Seismic time-invariant convolutional model, *Geophysics, 50,* 1244–1251.

Robinson, E.A. and Treitel, S., 1967, Principles of digital Wiener filtering, *Geophys. Prosp., 15,* 311–333.

Robinson, E.A. and Treitel, S., 1980, *Geophysical Signal Analysis,* Prentice-Hall.

Rosa, A.L.R. and Ulrych, T.J., 1991, Processing via spectral modeling, *Geophysics, 56,* 1244–1251.

Shtatland, E.S., 1991, Fractal stochastic models for acoustic impedance, an explanation of scaling or 1/f geology, and stochastic inversion: Reflections, 61st Ann. Internat. Mtg., Soc. Expl. Geophys., Expanded Abstracts, 1598–1601.

Todoeschuck, J.P., Jensen, O.G., and Labonte, S., 1990, Gaussian scaling noise model of seismic reflection sequences: Evidence from well logs, *Geophysics, 55,* 480–484.

Ulrych, T.J., 1971, Application of homomorphic deconvolution to seismology, *Geophsyics, 36,* 650–660.

Walden, A.T. and Hosken, J.W.J., 1985, An investigation of the spectral properties of primary reflection coefficients, *Geophys. Prosp., 33,* 400–435.

Wiggins, R., 1978, Minimum entropy deconvolution, *Geoexploration, 16,* 21–35.

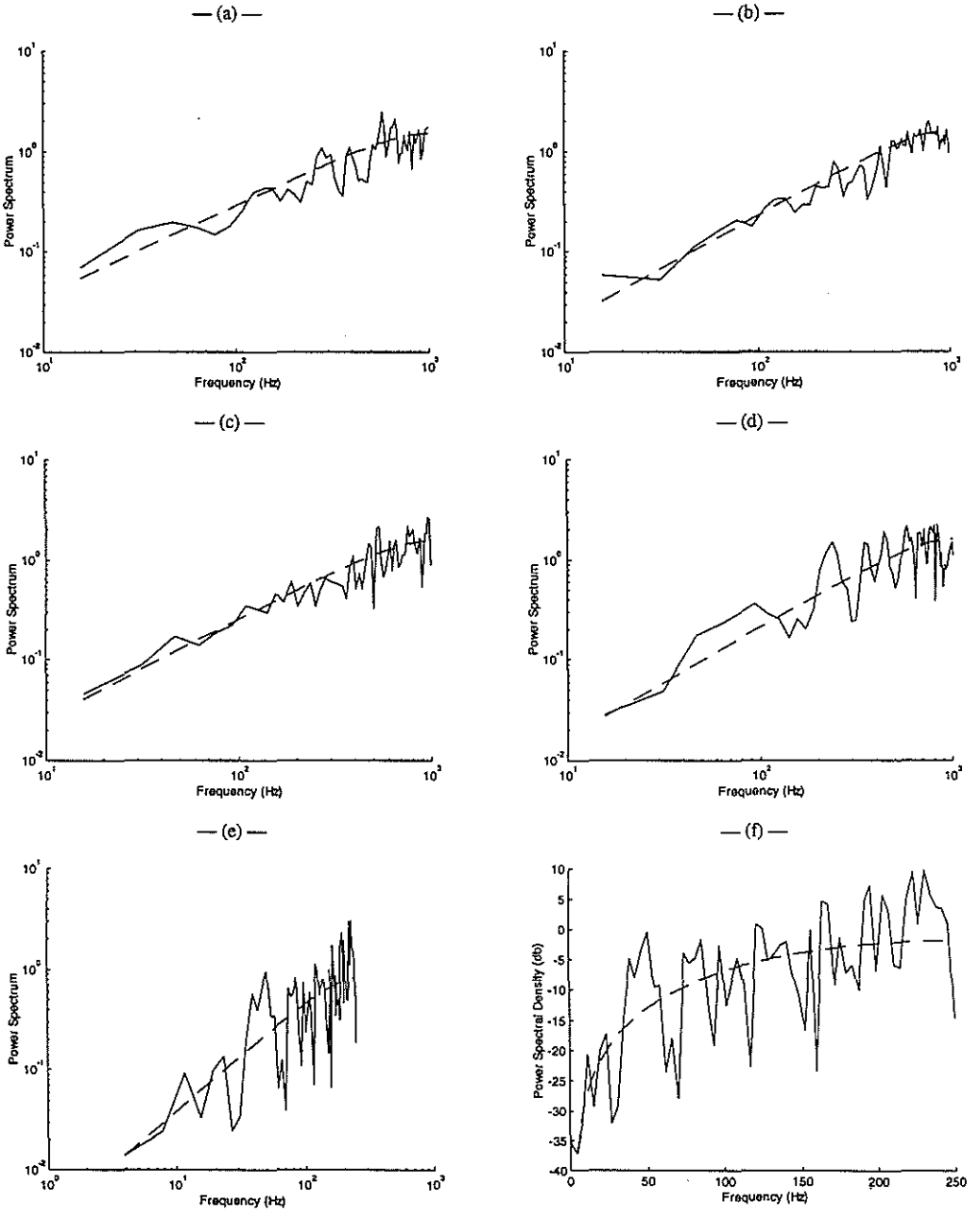

Figure 1: Power spectrum of reflectivity derived from well logs and the spectrum (dashed line) for the best-fitting fractionally integrated noise process: (a) well A (process order $= -0.45$), (b) well B (-0.53), (c) well C (-0.49), (d) well D at 0.5 ms sampling (-0.55), (e) well D at 2 ms sampling (-0.55), and (f) well D at 2 ms sampling shown in decibels.

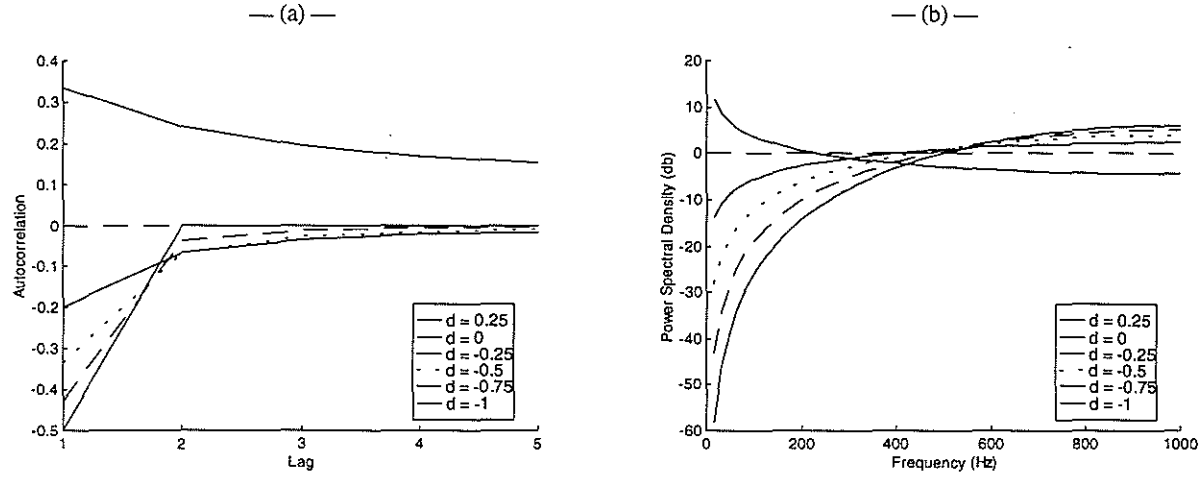

Figure 2: (a) Auto-correlation function and (b) power spectral density of fractionally integrated noise processes of various orders. Lag zero is not shown for the auto-correlation.

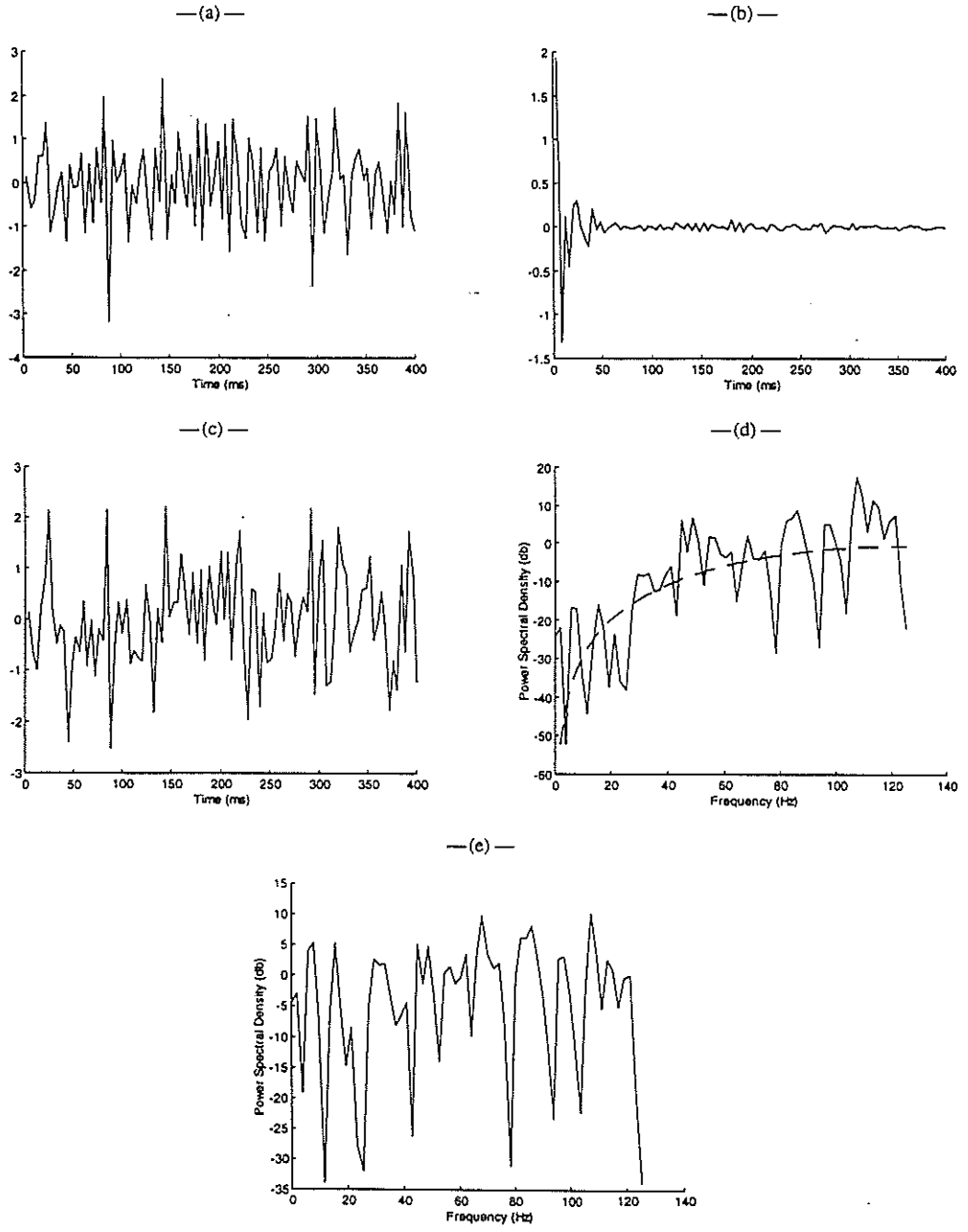

Figure 3: (a) 100-point realization of a reflectivity series, (b) its minimum-phase component, (c) its all-pass component, (d) power spectrum of full reflectivity and that of a fractionally integrated noise process of order -0.8 (dashed), and (e) power spectrum of the all-pass component of reflectivity.

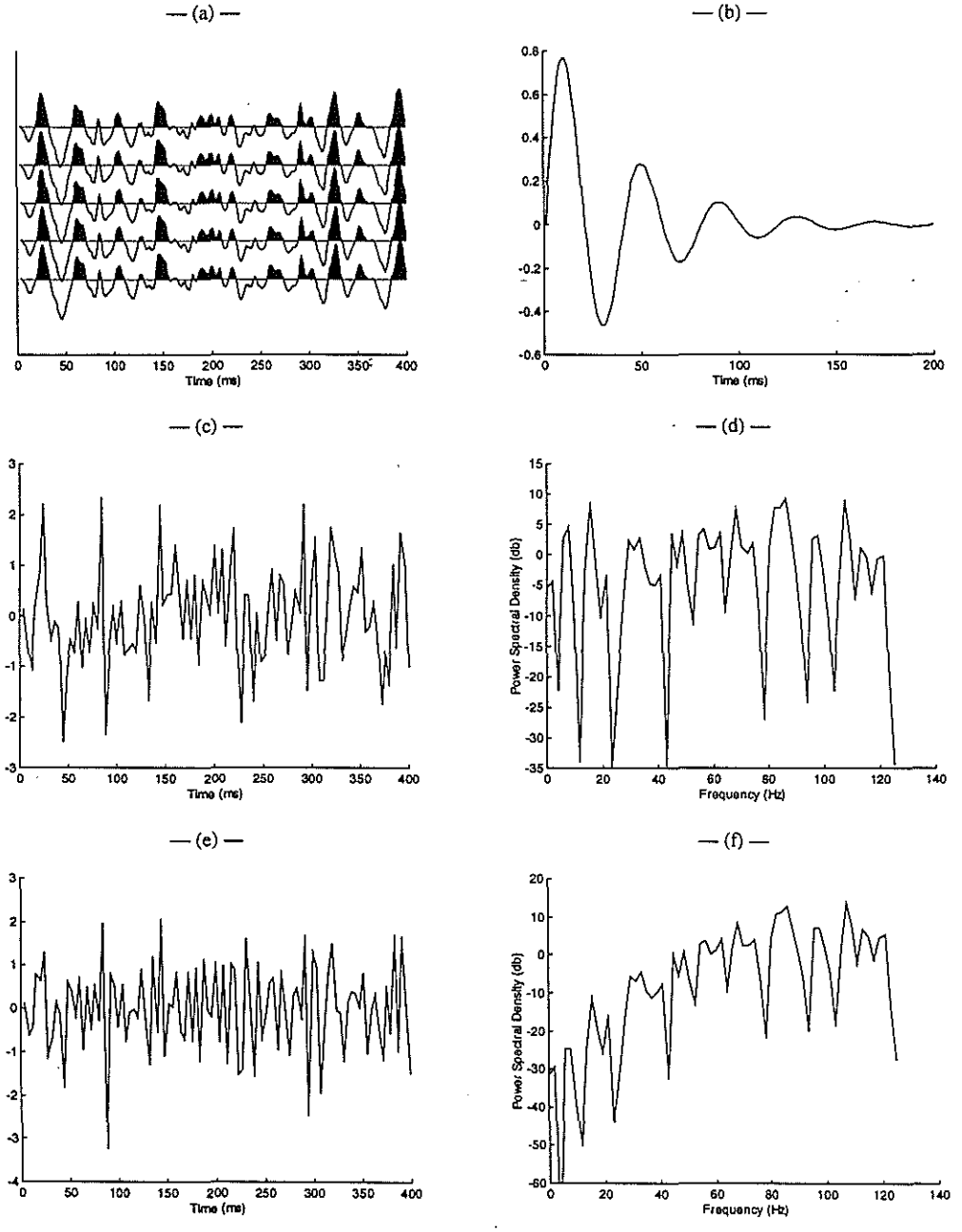

Figure 4: (a) Trace derived from original full reflectivity, (b) wavelet used to construct the trace, (c) reflectivity recovered from the trace using conventional deconvolution, (d) its power spectrum, (e) reflectivity recovered from the trace using a generalized deconvolution technique (spectral compensation filter), and (f) its power spectrum.

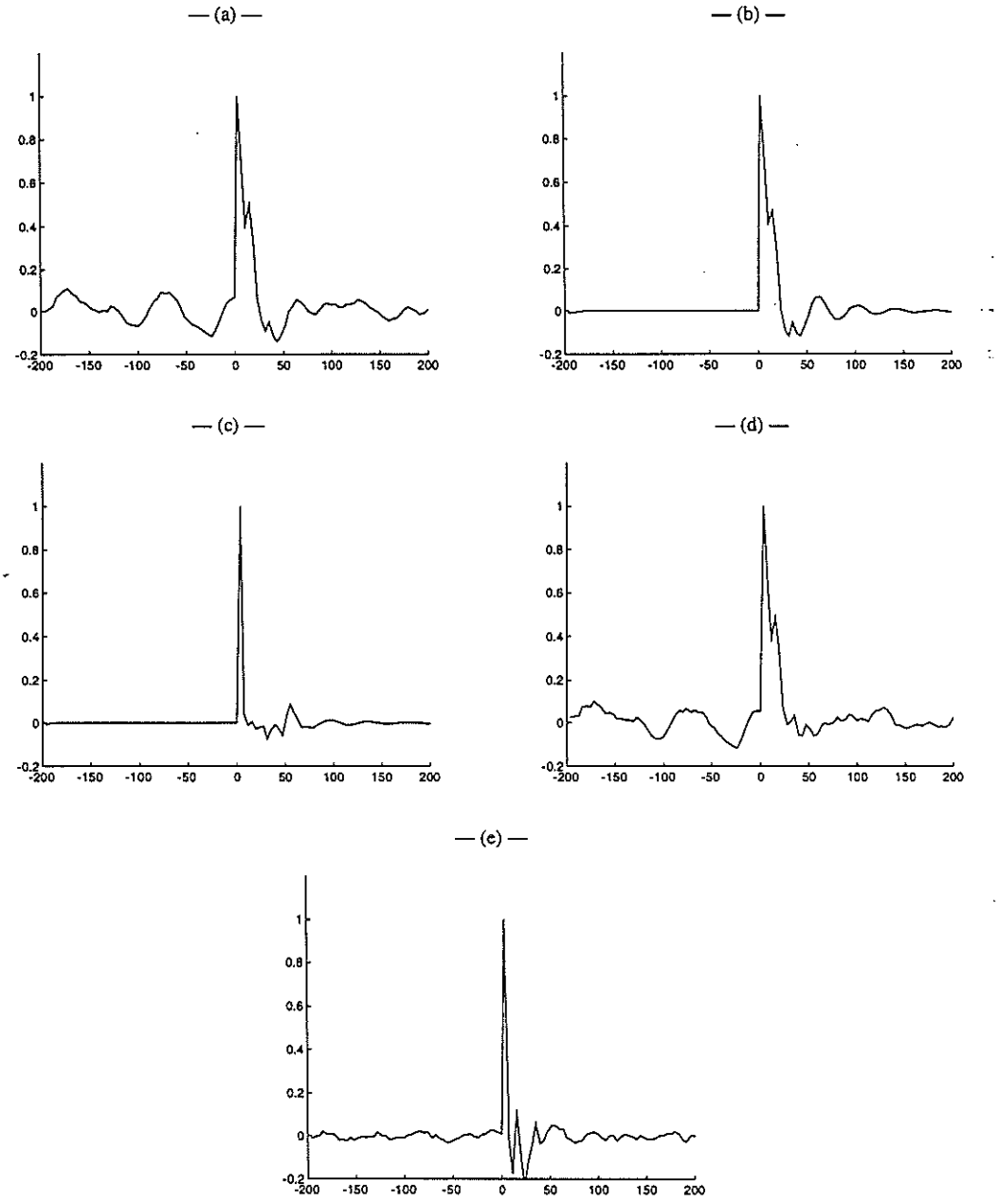

Figure 5: (a) Residual wavelet left by conventional deconvolution, (b) convolution of the conventional operator with the seismic wavelet ($f * w$), (c) performance of the conventional deconvolution filter as an inverse operator to the nonwhite component of the trace ($f * w * r_m$), (d) residual wavelet left after deconvolving the true reflectivity from the all-pass component (i.e. convolution of the all-pass component and the inverse of full reflectivity), and (e) residual wavelet left by the generalized deconvolution filter.

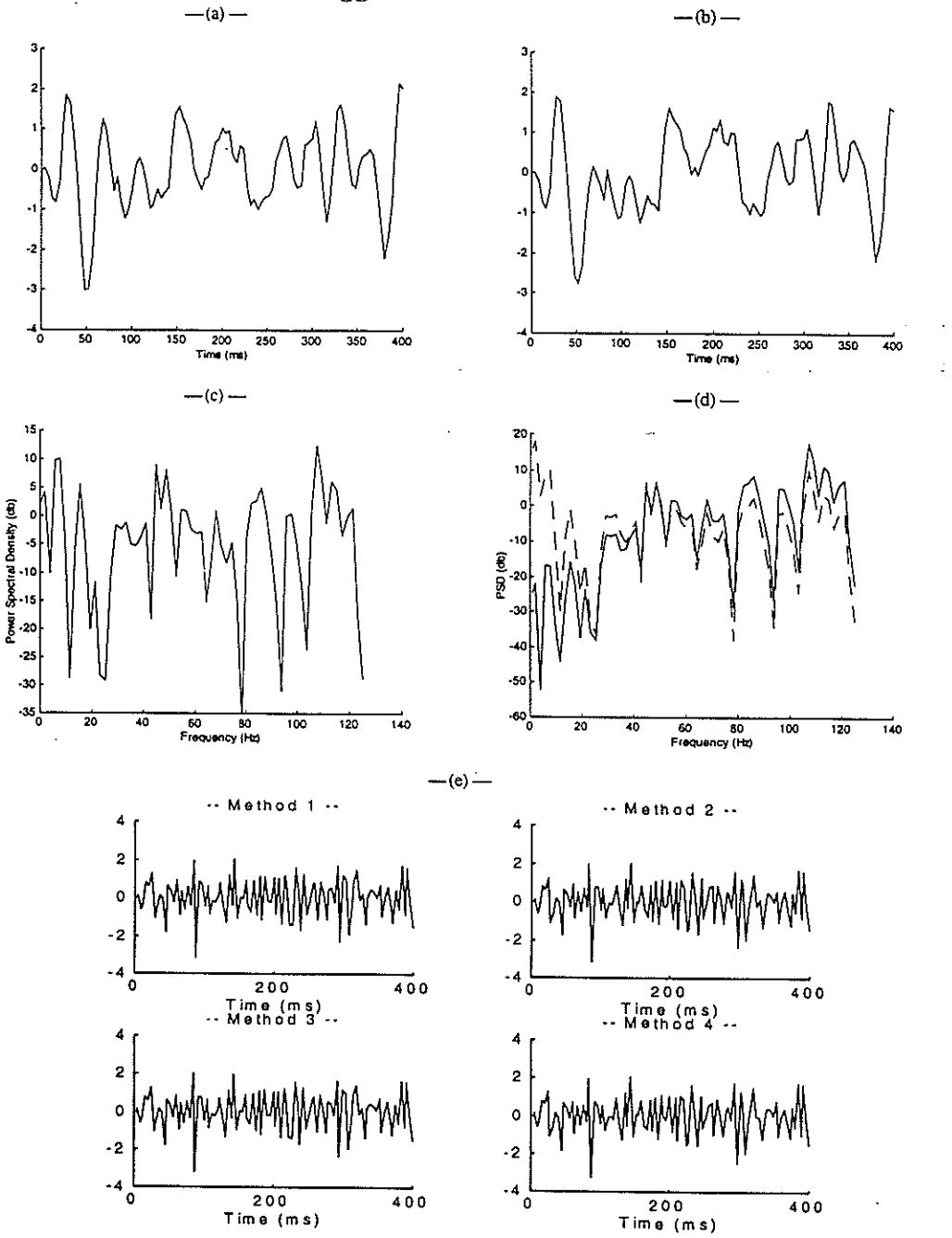

Figure 6: (a) Trace minus the minimum-phase component of reflectivity (i.e., convolution of the wavelet and all-pass component of reflectivity), (b) trace after application of the whitening filter, (c) power spectrum of reflectivity after application of the whitening filter, (d) power spectrum of reflectivity before and after (dashed) whitening in the frequency domain, and (e) comparison of the outputs of the four generalized deconvolution schemes.

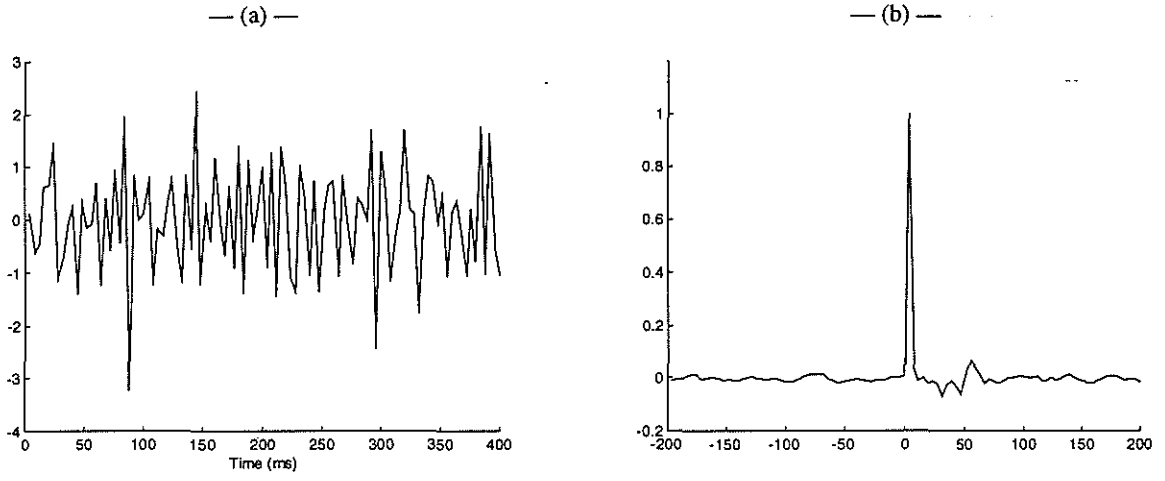

Figure 7: (a) Reflectivity recovered from the trace using a filter designed from the exact auto-correlation of reflectivity, and (b) residual wavelet left by that filter.

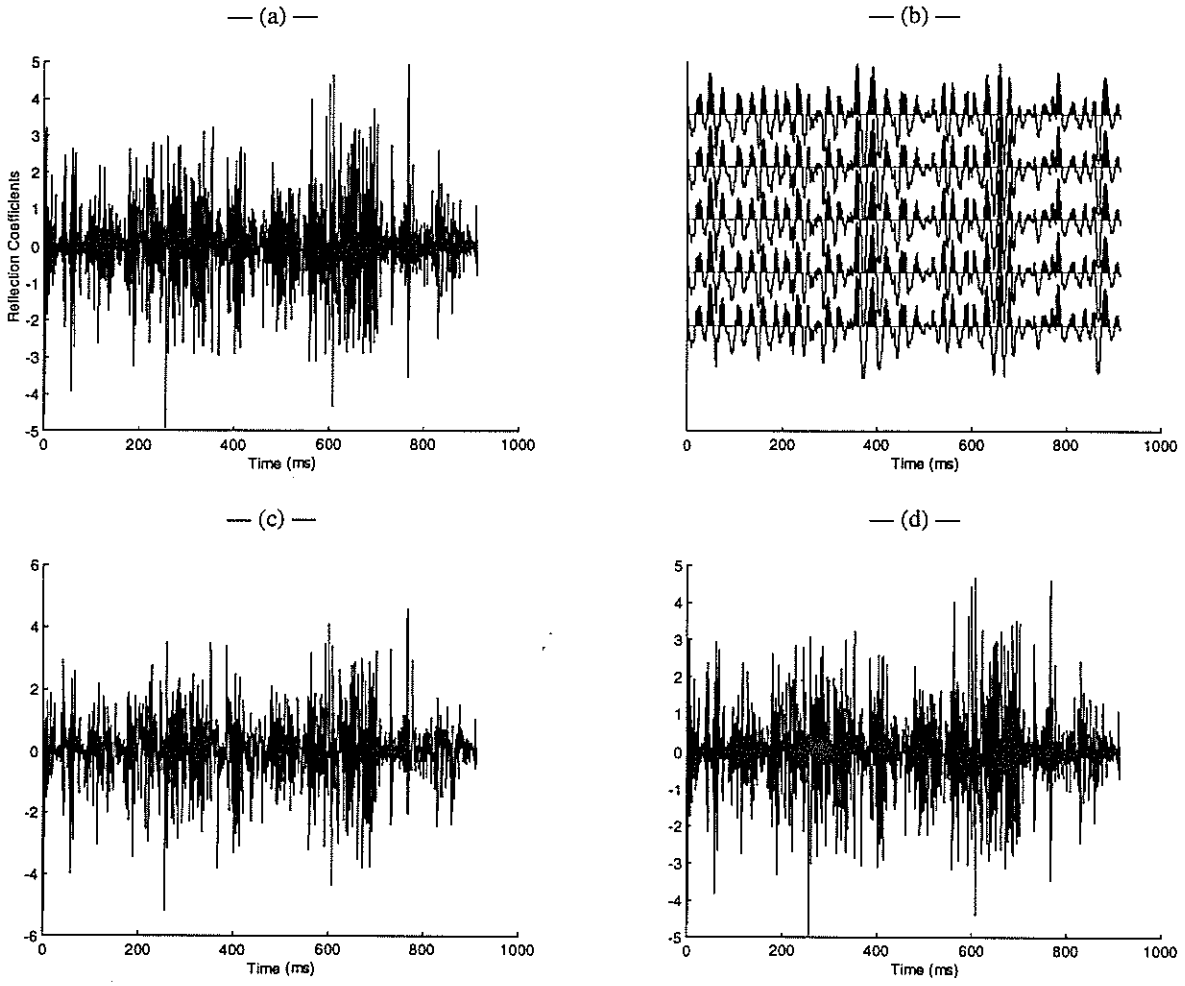

Figure 8: Well A: (a) reflection coefficients, (b) trace, (c) recovered reflection coefficients using conventional deconvolution, and (d) recovered reflection coefficients using a generalized deconvolution filter with a process order of -0.45.

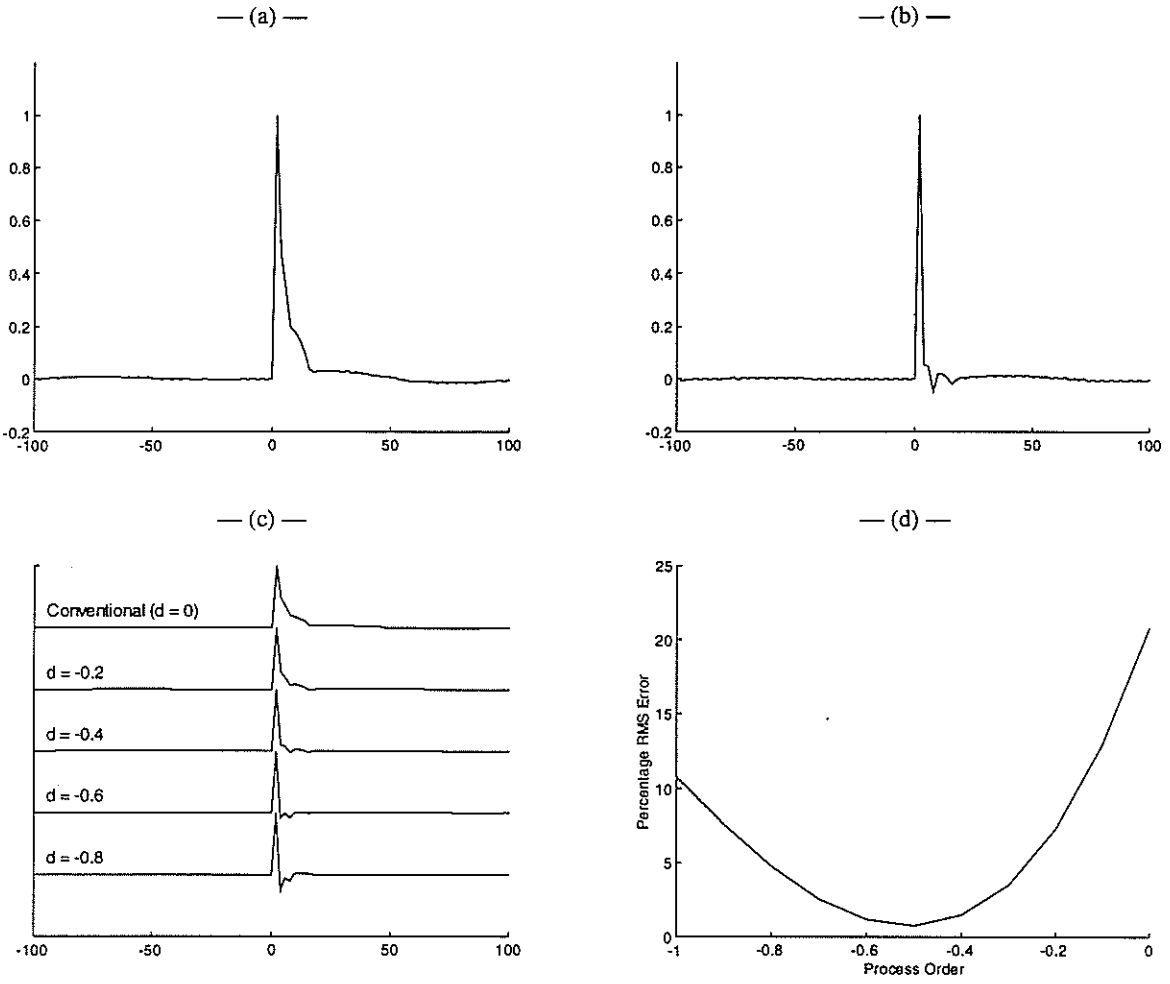

Figure 9: Well A: (a) residual wavelet left by conventional deconvolution, (b) residual wavelet left by a generalized deconvolution filter with a process order of -0.45, (c) residual wavelet left by generalized deconvolution filters of various process orders, and (d) RMS error for generalized deconvolution filters of various process orders plotted versus the process order.

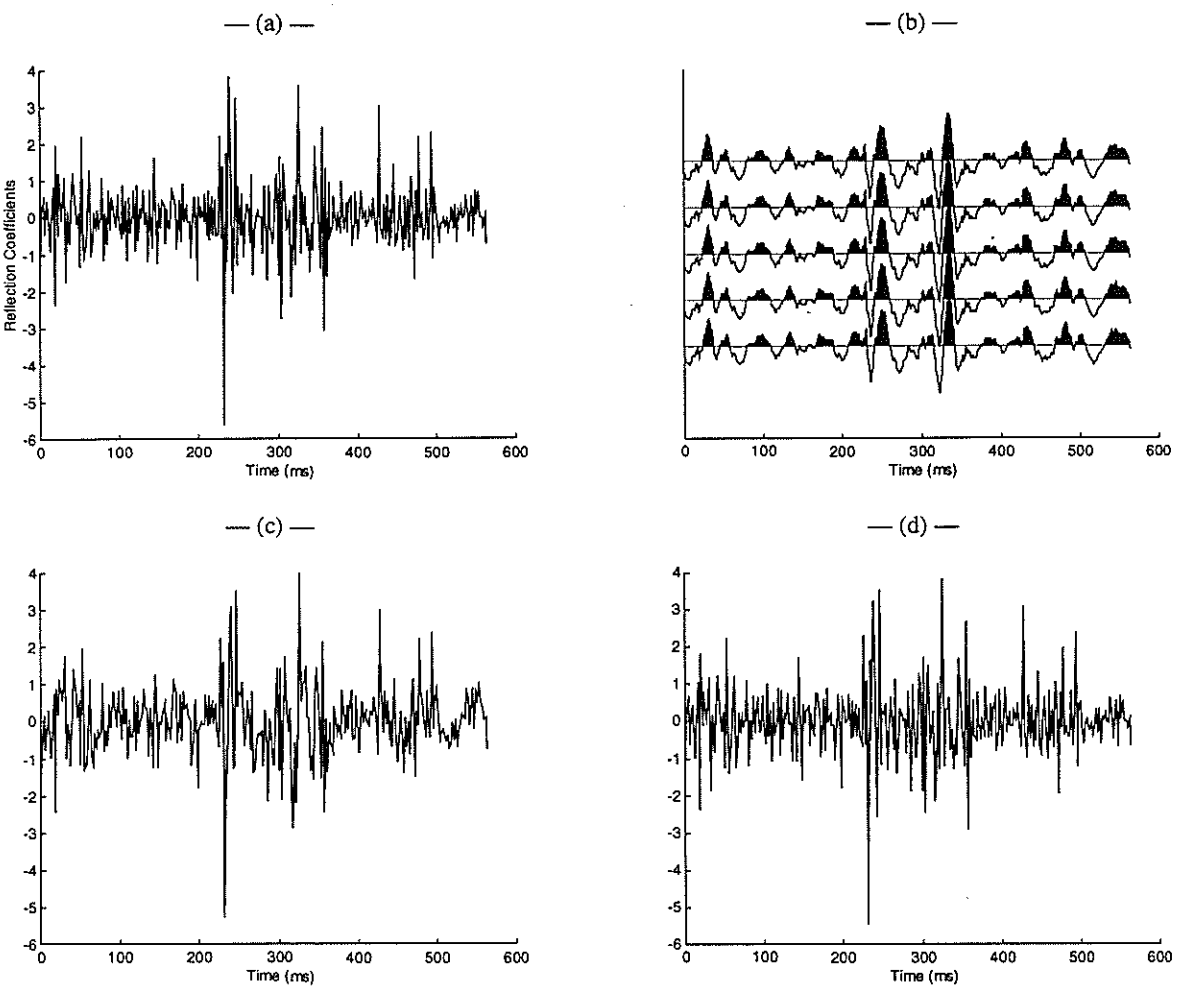

Figure 10: Well D: (a) reflection coefficients, (b) trace, (c) recovered reflection coefficients using conventional deconvolution, and (d) recovered reflection coefficients using a generalized deconvolution filter with a process order of -0.55.

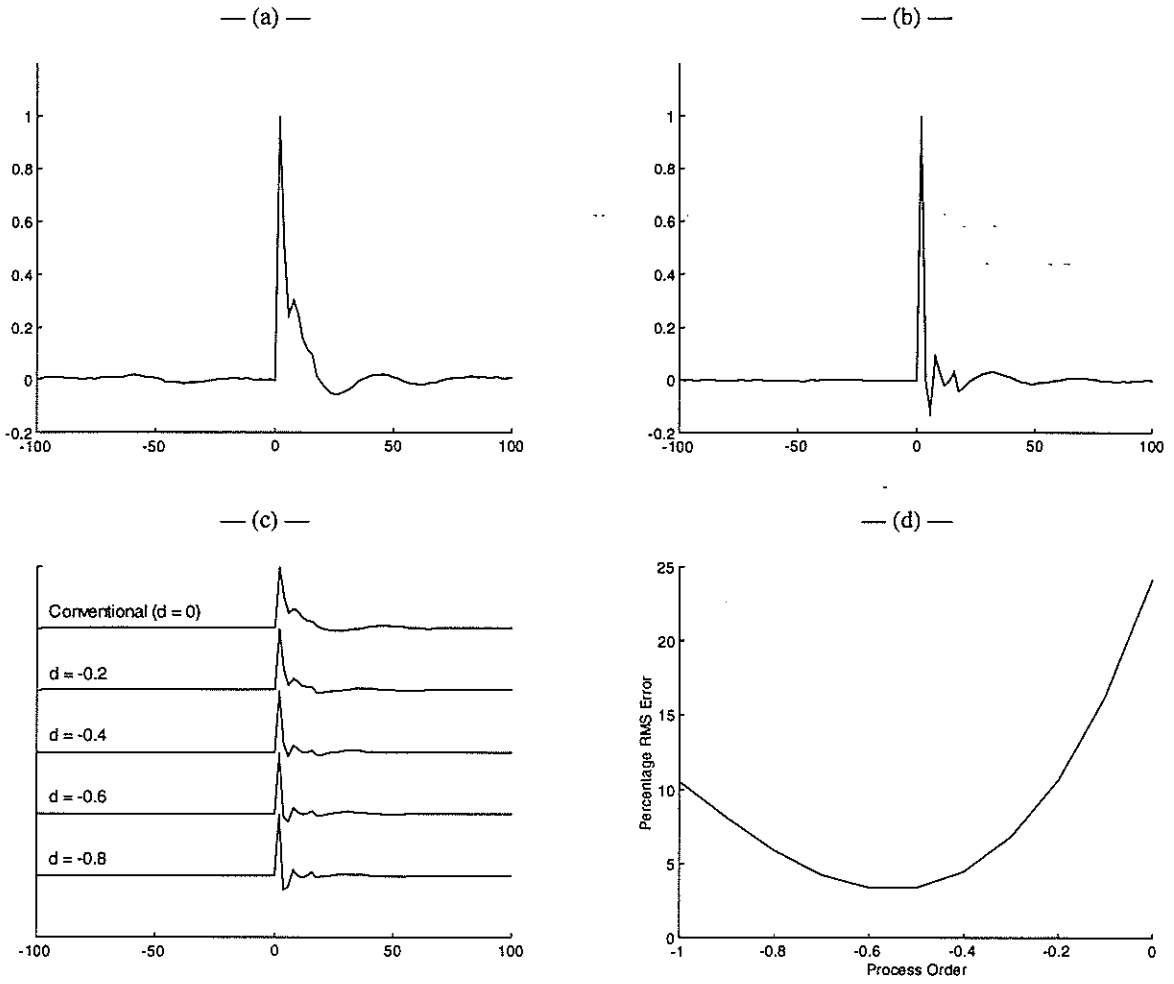

Figure 11: Well D: (a) residual wavelet left by conventional deconvolution, (b) residual wavelet left by a generalized deconvolution filter with a process order of -0.45, (c) residual wavelet left by generalized deconvolution filters of various process orders, and (d) RMS error for generalized deconvolution filters of various process orders plotted versus the process order.

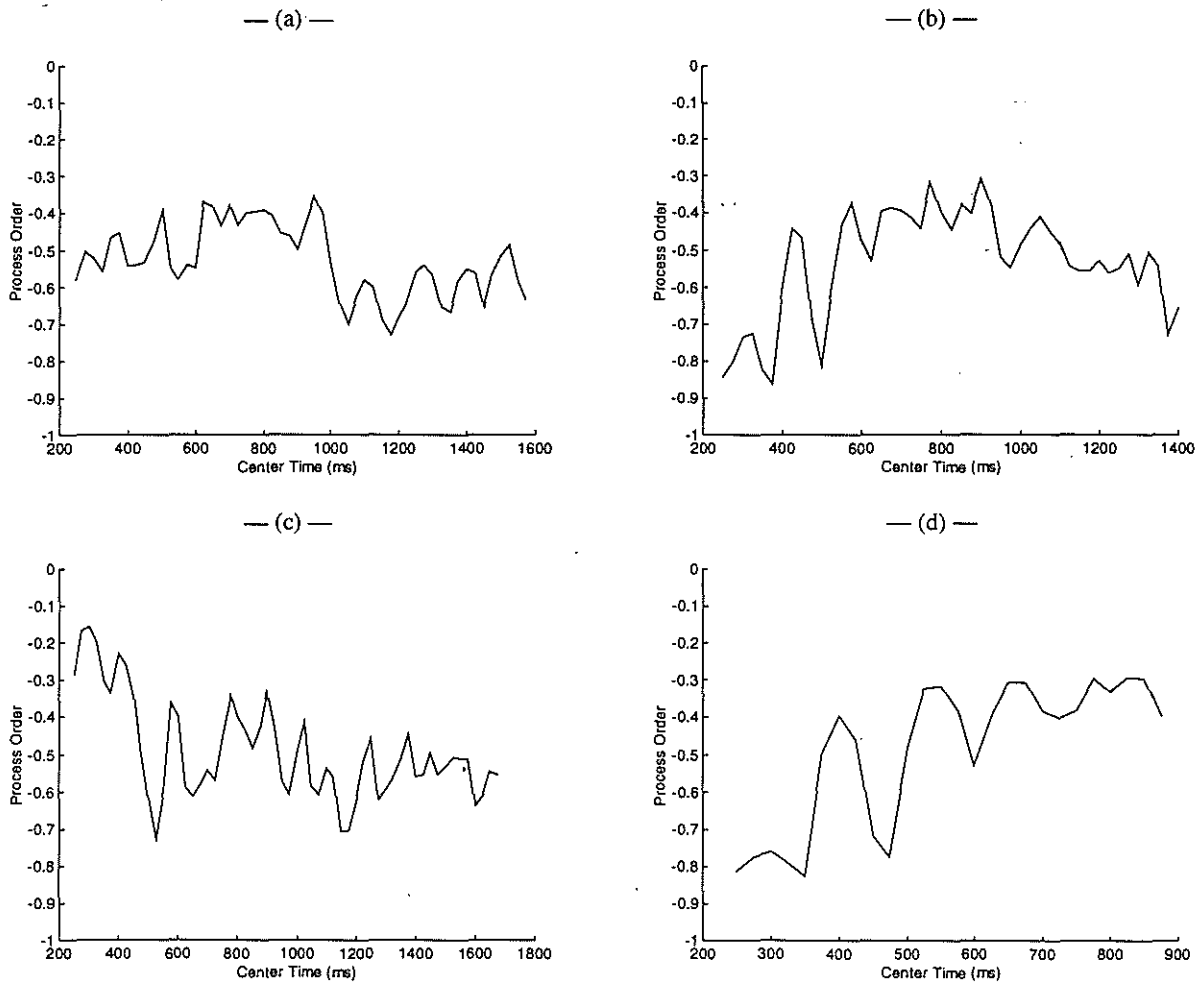

Figure 12: Order of the best-fitting fractionally integrated noise process for a 500-point sliding window along the wells whose power spectra appear in Figures 1a-d, plotted against the center point of the window: (a) well A, (b) well B, (c) well C, and (d) well D.